JCTC Journal of Chemical Theory and Computation

pubs.acs.org/JCTC Article

Exchange Repulsion in Quantum Mechanical/Effective Fragment Potential Excitation Energies: Beyond Polarizable Embedding

Claudia I. Viquez Rojas and Lyudmila V. Slipchenko*

Cite This: J. Chem. Theory Comput. 2020, 16, 6408−6417 Read Online

ACCESS | Metrics & More | Article Recommendations | Supporting Information

ABSTRACT: Hybrid quantum mechanical and molecular mechanical (QM/MM) approaches facilitate computational modeling of large biological and materials systems. Typically, in QM/MM, a small region of the system is modeled with an accurate quantum mechanical method and its surroundings with a more efficient alternative, such as a classical force field or the effective fragment potential (EFP). The reliability of QM/MM calculations depends largely on the treatment of interactions between the two subregions, also known as embedding. The polarizable embedding, which allows mutual polarization between solvent and solute, is considered to be essential for describing electronic excitations in polar solvents. In this work, we employ the QM/EFP model and extend the polarizable embedding by incorporating two short-range terms—a charge penetration correction to the electrostatic term and the exchange-repulsion term—both of which are modeled with one-electron contributions to the quantum Hamiltonian. We evaluate the accuracy of these terms by computing excitation energies across 37 molecular clusters consisting of biologically relevant chromophores surrounded by polar solvent molecules. QM/EFP excitation energies are compared to the fully quantum mechanical calculations with the configuration interaction singles (CIS) method. We find that the charge penetration correction diminishes the accuracy of the QM/EFP calculations. On the other hand, while the effect of exchange-repulsion is negligible for most $\pi\pi^*$ transitions, the exchange-repulsion significantly improves description of $n\pi^*$ transitions with blue solvatochromic shifts. As a result, addition of the exchange-repulsion term improves the overall accuracy of QM/EFP. Performances of QM/EFP models remain similar when excitation energies are modeled with cc-pVDZ and aug-cc-pVDZ basis sets.

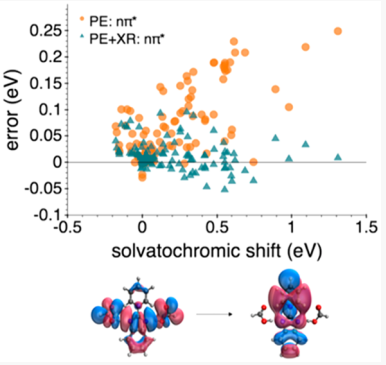

INTRODUCTION

A popular and efficient way to model the electronic properties of solvated systems is to use hybrid quantum mechanical and molecular mechanical methods (QM/MM).[1−5] In QM/MM the chemically relevant region is modeled with an appropriate *ab initio* method, while its surroundings are modeled with a force field. Various QM/MM methods[6−16] have been developed since the initial work of Warshel,[17] including multilayer methods such as ONIOM,[18−20] Truhlar MCMM methods,[21,22] and polarizable QM/MM for linear response methods by Kongsted and co-workers.[23−25] The Hamiltonian of the QM/MM system consists of three terms:

$$\hat{H} = \hat{H}_{QM} + \hat{H}_{MM} + \hat{H}_{QM/MM} \quad (1)$$

where H_{QM} and H_{MM} are the Hamiltonians of the QM and MM subsystems, respectively, and $H_{QM/MM}$ is the coupling term. Separation of the QM and MM subsystems, in principle, allows one to use any method for each part. The complexity of QM/MM methods varies from simple mechanistic embedding in which QM and MM systems do not interact, to electrostatic embedding where the MM system polarizes the QM system, and to polarization embedding in which QM and MM systems polarize each other self-consistently (Figure 1).[26] In this work we take a step further by including exchange-repulsion interactions between the QM and MM subsystems into the $H_{QM/MM}$ coupling Hamiltonian.

Our methodology is based on the effective fragment potential (EFP) method,[27−35] a model designed for evaluating noncovalent interactions in chemical and biological systems. The EFP method is one of a few available general polarizable potentials, with AMOEBA,[36] SIBFA,[37,38] and several others[23−25,39,40] becoming also increasingly popular. In EFP the surroundings are fragmented, with each fragment corresponding to a small molecule or a section of a macromolecule.[41] The full interaction energy of the chemical system is described as the sum of Coulomb, polarization, dispersion, and exchange-repulsion terms. The Coulomb term represents the interaction between fragments due to their static electronic densities, represented with a distributed multipole expansion truncated at octupoles.[42] The polarization term describes energy lowering due to the redistribution of the electronic density on a fragment

Received: November 21, 2019
Published: August 10, 2020

https://dx.doi.org/10.1021/acs.jctc.9b01156
J. Chem. Theory Comput. 2020, 16, 6408−6417

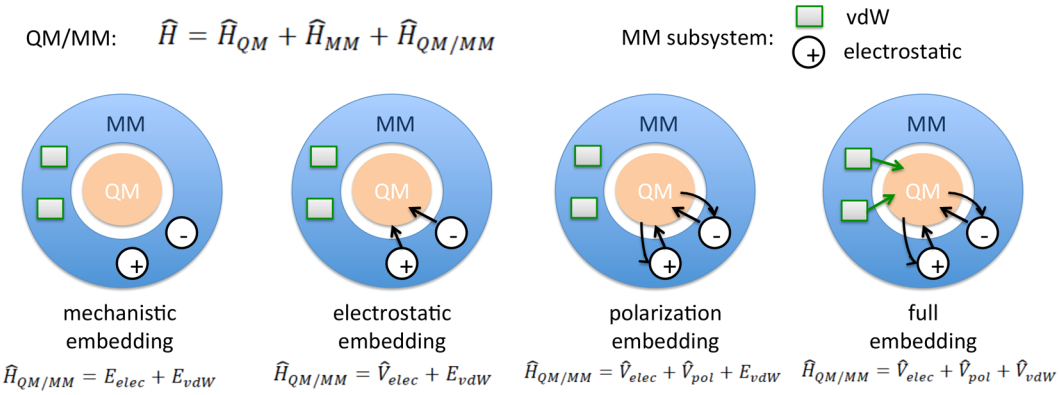

Figure 1. Hierarchy of QM/MM approximations. In mechanistic embedding, all interactions between QM and MM subsystems are described at the MM level (classically). In electrostatic embedding the MM subsystem polarizes the QM region through the electrostatic operator $\hat{V}_{elec}$ in the QM/MM Hamiltonian. In polarization embedding the QM subsystem back-polarizes the classical subsystem with the $\hat{V}_{pol}$ operator in $\hat{H}_{QM/MM}$. Van der Waals interactions are also described quantum mechanically ($\hat{V}_{vdw}$) in the full embedding QM/MM.

consequent of the electric field of other fragments. In EFP, polarization is computed as an interaction of induced dipoles, which appear when an electric field acts on distributed anisotropic polarizability tensors, with the electric field due to other fragments. The induced dipoles are computed self-consistently, such that the polarization term includes many-body effects.[35] The dispersion term accounts for London forces between fragments and is modeled as the first R^{-6} term with C_6 coefficients computed using distributed dynamic polarizabilities of the fragments.[43] The exchange repulsion accounts for the antisymmetry of the wave functions of the fragments and is modeled using interfragment kinetic and overlap integrals, as well as the Fock matrices from the fragments.[44]

In previous applications of the QM/EFP methodology,[41,45−50] the interaction between the fragments and the QM region was typically described using the Coulomb and polarization terms, known as polarizable embedding and represented with the following coupling Hamiltonian $H_{QM/EFP}$:

$$\hat{H}_{QM/EFP} = \langle p|\hat{V}^{coul} + \hat{V}^{pol}|q\rangle p^{\dagger} q \tag{2}$$

where p and q represent the atomic orbitals in the QM region. In polarizable embedding, the EFP environment responds to electron density changes in the QM region. It has been extensively shown that polarizable embedding is essential for predicting accurate electronic and redox properties of chromophores in solvents and biological environments.[51−54]

Previous methodological developments aimed at extending the QM/EFP models and the Hamiltonian from eq 2 to account for short-range terms. For example, the electrostatics term in QM/EFP was modified to include a charge-penetration correction.[30,41] The exchange-repulsion and dispersion QM/EFP terms have also been developed.[32,55−57] However, to date, polarizable embedding remains the most common scheme, while the effects of the other terms on the electronic properties of a solute have not been investigated in detail.

In this work, we build upon the previous methodological developments of QM/EFP. We explore the effects of charge-penetration and exchange-repulsion coupling terms on the electronic excitation energies of biologically relevant chromophores surrounded by small clusters of water, ammonia, methanol, and formic acid. The initial structures were adapted from the recent work of Zech et al.[58] Complexes with charged chromophores or those with solvent molecules rather than water, ammonia, methanol, and formic acid were excluded from consideration. The resulting data set included 37 structures of neutral clusters. We considered configuration interaction singles (CIS) as a reference method for various QM(CIS)/EFP embedding schemes including the charge-penetration and exchange-repulsion components. We identified the best embedding scheme as the one showing the smallest mean and variance with respect to the QM reference. We also examined how the QM/EFP errors correlate with a type of the electronic transition and the values of solvatochromic shifts.

METHODS

In this work we consider several variants of the QM/EFP models for the electronic excited states. The basic polarizable embedding model has been described in detail previously[29,32,34,47] and is defined as

$$E_{PE,0} = \langle \Psi_0|\hat{H}_{QM} + \hat{V}^{coul} + \hat{V}_0^{pol}|\Psi_0\rangle + E_0^{pol} + E_{QM/EFP,0}^{disp} + E_{EFP}^{coul} + E_{EFP}^{disp} + E_{EFP}^{ex\text{-}rep} \tag{3}$$

where Ψ_0 is the ground state electronic wave function of the QM region. The last three terms of the sum account for electrostatics, dispersion, and exchange-repulsion interactions between the EFP fragments and are unaffected by the QM wave function. Subscripts "0" in the polarization energy of the QM/EFP system E_0^{pol} and in the polarization perturbation to the quantum Hamiltonian $\hat{V}_0^{pol}$ indicate that induced dipoles of the fragments are converged to full consistency with the ground state wave function Ψ_0 of the QM subsystem.[46,47] Dispersion energy between the QM and EFP subsystems $E_{QM/EFP,0}^{disp}$ is a perturbative energy correction computed based on the ground state wave function of the quantum region.[55] In the present formulation, the EFP solvent response to electronic excitations in the QM region is not accounted for, such that the last five terms in eq 3 do not affect the properties of the electronic excited states.

The electrostatic contribution to the QM Hamiltonian due to a multipole expansion of a fragment is given by[28,30]

$$\hat{V}_k^{coul} = q_k T(r_k) - \sum_a^{x,y,z} \mu_a^k T_a(r_k) + \frac{1}{3}\sum_{a,b}^{x,y,z} \Theta_{a,b}^k T_{a,b}(r_k) - \frac{1}{15}\sum_{a,b}^{x,y,z} \Omega_{a,b,c}^k T_{a,b,c}(r_k) \tag{4}$$

https://dx.doi.org/10.1021/acs.jctc.9b01156
J. Chem. Theory Comput. 2020, 16, 6408−6417

Table 1. QM/EFP Embedding Schemes

label	description	QM/EFP Hamiltonian
PE	polarizable embedding	$\langle p\lvert\hat{V}^{\text{coul}} + \hat{V}^{\text{pol}}\rvert q\rangle p^{\dagger} q$
PE + XR	PE + exchange repulsion	$\langle p\lvert\hat{V}^{\text{coul}} + \hat{V}^{\text{pol}} + \hat{V}^{\text{ex-rep}}\rvert q\rangle p^{\dagger} q$
PE + S	PE + charge-penetration screen	$\langle p\lvert\hat{V}^{\text{coul}}_{\text{chpen}} + \hat{V}^{\text{pol}}\rvert q\rangle p^{\dagger} q$
PE + SXR	PE + charge-penetration screen + exchange repulsion	$\langle p\lvert\hat{V}^{\text{coul}}_{\text{chpen}} + \hat{V}^{\text{pol}} + \hat{V}^{\text{ex-rep}}\rvert q\rangle p^{\dagger} q$

where q, μ, Θ, and Ω are the net charge, dipole, quadrupole, and octupole at point k. T represents the electrostatics tensors of zero, first, second, and third order, and r_k is the distance between the expansion point k and the coordinate of an electron in the QM region.

The polarization contribution to the QM Hamiltonian is as follows:[30]

$$\hat{V}_p^{\text{pol}} = \frac{1}{2}\sum_a^{x,y,z} \frac{(\mu_a^p + \tilde{\mu}_a^p)a}{r_p^{\,3}} \tag{5}$$

where μ_a^p and $\tilde{\mu}_a^p$ represent the induced dipole and conjugated induced dipole at the distributed polarizability point p. r_p refers to the distance between the polarizability point of an effective fragment and an electron of the QM region, and a is the x, y, or z component of the distance r_p. The induced dipoles are converged until self-consistency with each other and with the electronic wave function.

Response of the polarizable environment to changes in the electronic wave function upon electronic excitation can be further accounted for either in state-specific or linear response fashion, as has been shown by several research groups.[59−63] Perturbative state-specific corrections to the excitation energies due to polarizable environment were also explored by us and others.[46,64−66] Generally, inclusion of explicit coupling between environment polarization and the electronic excited state leads to small but systematic lowering of excitation energies. However, in this work we utilize a zero-order scheme of eq 3 without inclusion of explicit excited-state polarization corrections.

In this work we consider two modifications to the basic polarizable embedding scheme of eq 3. The first modification is electrostatic screening achieved by Gaussian smearing of the charges on the effective fragments. With this modification, the electrostatic potential of eq 4 becomes[30,41]

$$\begin{aligned}\hat{V}^{\text{coul}}_{k,\text{chpen}} = {} & [q_k^{\text{nuc}} + q_k^{\text{elec}}(1 - \exp(-\alpha_k r_k^{\,2}))]T(r_k) \\ & - \sum_a^{x,y,z} \mu_a^k T_a(r_k) + \frac{1}{3}\sum_{a,b}^{x,y,z} \Theta_{a,b}^k T_{a,b}(r_k) \\ & - \frac{1}{15}\sum_{a,b}^{x,y,z} \Omega_{a,b,c}^k T_{a,b,c}(r_k)\end{aligned} \tag{6}$$

where q_k^{nuc} and q_k^{elec} are nuclear and electronic components of the net charge q_k on a fragment's expansion point k; α_k is the charge-penetration parameter at point k obtained during the parameter-determining step by a fit of the screened multipole potential to the Hartree−Fock potential around the fragment.[67] The goal of the charge-penetration screening is to improve accuracy of the electrostatic interactions at close separations between the QM and EFP regions.

The second modification explored in this work is extending the polarizable embedding Hamiltonian to the exchange-repulsion term. To reduce the computational cost associated with this term, we utilized a parametrized version, in which exchange repulsion between the QM region and EFP fragments is modeled using Gaussian functions positioned at the centroids j of the localized molecular orbitals (LMOs) of each fragment:[56]

$$\hat{V}_j^{\text{ex-rep}} = \beta_j \exp(-\gamma_j r_j^{\,2}) \tag{7}$$

where γ_j and β_j are parameters determined for each unique type of LMO; r_j specifies the distance between electron of the QM region and the LMO centroid. Exchange-repulsion parameters γ_j and β_j for main bonding patterns including single, double, triple, and aromatic bonds between carbon, oxygen, nitrogen, and hydrogen atoms were determined in ref 56 by minimizing the exchange-repulsion and total energy differences with EFP and SAPT0[68,69] calculations. The exchange-repulsion term utilized in this work is similar in spirit to the reminder term in the QM/EFP1 water model.[30] Similarly to the reminder term in QM/EFP1, exchange repulsion in QM/EFP accounts for some of charge-transfer effects and other higher-order interaction terms between QM and EFP regions. Advantages of using the fitted QM/EFP exchange-repulsion term are in its straightforward extension to analytic gradients and electronic excited states, low computational cost (indeed, negligible for a typical QM/EFP setup), and simplicity of formulation, allowing fast development of analogue functionality in electronic structure packages interfaced with the EFP software library LibEFP.[70,71] Contrarily, the alternative rigorous formulation of the QM/EFP exchange-repulsion term[32,57] requires calculations of two-electron integrals between QM and EFP regions, which makes it more computationally expensive and not easily extendable to electronic excited states. The fitted QM/EFP exchange-repulsion term utilized in this work is similar to but more simplistic than atomic all-electron pseudopotentials introduced in ref 72 and electrostatic repulsive potentials from ref 73. Alternatively, Pauli repulsion can be accounted for using overlap or exchange integrals between solute and solvent densities, which was explored in the context of the polarizable density embedding (PDE) and QM/MM models.[74−78] Fragment exchange potentials were also recently introduced in the context of fragment-based methods.[79]

We consider the performances of four QM/EFP schemes based on polarizable embedding, which are summarized in Table 1. These include the basic polarizable embedding scheme (PE), polarizable embedding with inclusion of charge-penetration screening (PE + S), a scheme with an added exchange-repulsion term (PE + XR), and a scheme with both exchange-repulsion and charge-penetration contributions (PE + SXR).

COMPUTATIONAL DETAILS

In this work we considered 37 neutral molecular systems; each consisted of one of the chromophores shown in Figure 2

https://dx.doi.org/10.1021/acs.jctc.9b01156
J. Chem. Theory Comput. 2020, 16, 6408−6417

surrounded by molecules of water, ammonia, methanol, or formic acid. The starting optimized structures were obtained from ref 58.

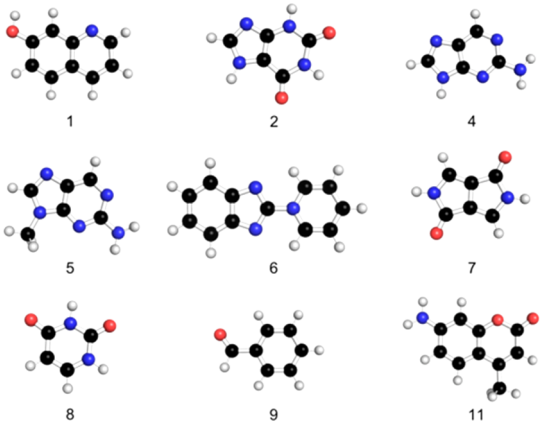

Figure 2. Chromophores studied in this work: (1) 7-hydroxyquinoline, (2) xanthine, (4) 2-aminopurine, (5) 7-methyl-2-aminopurine, (6) pyridiniumyl benzimidazolide, (7) diketopyrrolopyrrole, (8) uracil, (9) benzaldehyde, and (11) 7-amino-4-methylcoumarin. Adapted from ref 58. Copyright 2018 American Chemical Society.

All excitation energies were computed in the GAMESS quantum chemistry package.[80,81] The following six calculations were performed on each system: (i) CIS/cc-pVDZ calculation on the gas-phase chromophore; (ii) CIS/cc-pVDZ calculation on the full system; (iii)−(vi) QM/EFP calculations corresponding to schemes described in Table 1. In all QM/EFP calculations, the QM region consisted only of the chromophore and was also modeled at the CIS/cc-pVDZ level of theory. Each solvent molecule was represented by an effective fragment. The EFP parameters for the fragments were calculated using a hybrid basis: 6-31+G(d) for electrostatics and charge-penetration parameters and 6-311++G(3df,2p) for all other components. The parameters for the QM/EFP exchange-repulsion term are taken from ref 56.

From each single-point-energy calculation, we obtained the lowest 15 excitation energies. To match the QM/EFP excitations to the full-system excitations we considered (1) the molecular orbitals corresponding to the leading transition, (2) the magnitude of the oscillator strength, and (3) the magnitude of the largest transition dipole component. The first criterion was satisfied if both transitions involved the same orbitals, which were matched visually and based on the scalar product of the orbital expansion coefficients. The second and third criteria were applied only to transitions with the oscillator strengths larger than 0.1 and were satisfied when the differences between the oscillator strengths and the largest components of the transition dipole between excitations were less than 25%.

To evaluate the performance of each scheme, we computed excitation energy errors as

$$E_{\text{error}} = E_{\text{QM/EFP}} - E_{\text{full}} \tag{8}$$

where, for a particular electronic transition, E_{full} is the corresponding CIS excitation energy for the full system. We then compared the error distribution across schemes. For the best two schemes, we also compared the mean absolute error (MAE) for different transition types and examined the dependence of the errors on solvatochromic shifts E_{shift}, defined as

$$E_{\text{shift}} = E_{\text{full}} - E_{\text{gas}} \tag{9}$$

where E_{gas} is an excitation energy in the gas-phase (isolated) chromophore.

Analogue analysis was also performed for the five lowest excited states of each molecular system.

The electronic excitations were classified as $\pi\pi^*$ or $n\pi^*$ based on the molecular orbitals corresponding to the leading transition. Additionally, the excitations were characterized based on whether they involved partial charge transfer to or from solvent. For this purpose, additional CIS calculations that involved analysis of charge distribution and natural transition orbital[82] (NTO) pairs were performed on each full system in the Q-Chem electronic structure software.[83] NTO calculations provided us with the main electron−hole pair for each transition. Mülliken population analysis was conducted on the attachment and detachment portions of the difference electronic density. A transition was considered to possess a charge transfer character if, according to the Mülliken population analysis, over 0.01 of the hole or electron charge was located on the solvent.

Additional calculations for the PE and PE + XR schemes were performed in aug-cc-pVDZ basis. In this case, five lowest excitations of 25 molecular structures were analyzed. EFP parameters for these calculations were the same as described above. The only difference in the setup for this analysis was that the orbitals for these excitations were matched only visually.

RESULTS AND DISCUSSION

Figure 3 shows error distributions for each QM/EFP scheme with respect to fully quantum calculations for 15 lowest excited

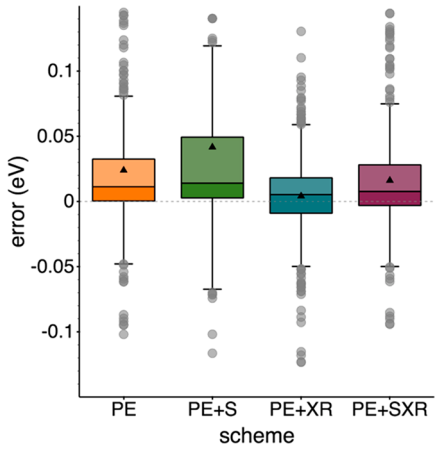

Figure 3. Error distribution for each QM/EFP scheme. Not all outliers are shown. Each box contains 50% of the data, 25% below the median (opaque box) and 25% above it (semitransparent box). The bottom whisker is computed as q1 − 1.5·IQR and the top as q3 + 1.5·IQR, where q1 is the first quartile, q3 is the third quartile, and the interquartile range (IQR) is their difference. Black triangles represent the means for each scheme.

states in 37 molecular systems. This information is also provided in the upper portion of Table 2. Positive errors mean that QM/EFP excitation energies are overestimated (shifted toward blue). On average, the basic PE scheme tends to overestimate excitation energies, with a mean absolute error (MAE) of 0.035 eV and a signed mean error of 0.024 eV. Figure 3 shows that adding the charge-penetration correction to the electrostatics term (PE + S) results in a broader error distribution skewed to the blue region. In other words, the excitation

https://dx.doi.org/10.1021/acs.jctc.9b01156
J. Chem. Theory Comput. 2020, 16, 6408−6417

Table 2. Signed Mean Errors (SMEs), Standard Deviations (STDs), and Mean Absolute Errors (MAEs) in Electronvolts for All Considered Excitations and Separate MAEs for $\pi\pi^*$ and $n\pi^*$ Excitations[a]

scheme	QM basis	no. of excitations[b]	states	SME	STD	MAE	$\pi\pi^*$ MAE	$n\pi^*$ MAE
PE	cc-pVDZ	375	1−15	0.024	0.052	0.035	0.018	0.069
PE + S	cc-pVDZ	298	1−15	0.042	0.086	0.052	0.020	0.110
PE + XR	cc-pVDZ	380	1−15	0.004	0.034	0.023	0.018	0.022
PE + SXR	cc-pVDZ	370	1−15	0.016	0.050	0.031	0.016	0.049
gas[c]	cc-pVDZ	286	1−15	−0.094	0.280	0.172	0.136	0.245
PE	cc-pVDZ	141	1−5	0.026	0.052	0.034	0.018	0.073
PE + S	cc-pVDZ	132	1−5	0.047	0.087	0.052	0.020	0.124
PE + XR	cc-pVDZ	140	1−5	0.001	0.025	0.017	0.018	0.016
PE + SXR	cc-pVDZ	139	1−5	0.016	0.038	0.024	0.015	0.047
gas[c]	cc-pVDZ	118	1−5	−0.106	0.268	0.184	0.126	0.298
PE	aug-cc-pVDZ	87	1−5	0.010	0.104	0.048	0.020	0.065
PE + XR	aug-cc-pVDZ	88	1−5	−0.024	0.065	0.032	0.021	0.013
gas[b]	aug-cc-pVDZ	78	1−5	−0.070	0.242	0.169	0.106	0.261
PE	aug-cc-pVDZ	58	1−5[d]	0.011	0.063	0.031	0.020	0.065
PE + XR	aug-cc-pVDZ	59	1−5[d]	−0.008	0.048	0.019	0.021	0.013
gas[c]	aug-cc-pVDZ	60	1−5[d]	−0.059	0.236	0.150	0.106	0.261

[a]Errors are computed as QM/EFP excitation energy − full QM excitation energy. [b]Number of excitations that could be matched between full QM and QM/EFP or gas phase calculations. [c]Gas phase values correspond to the negative of the solvatochromic shift. [d]Statistics excludes $\pi \rightarrow$ Rydberg excitations.

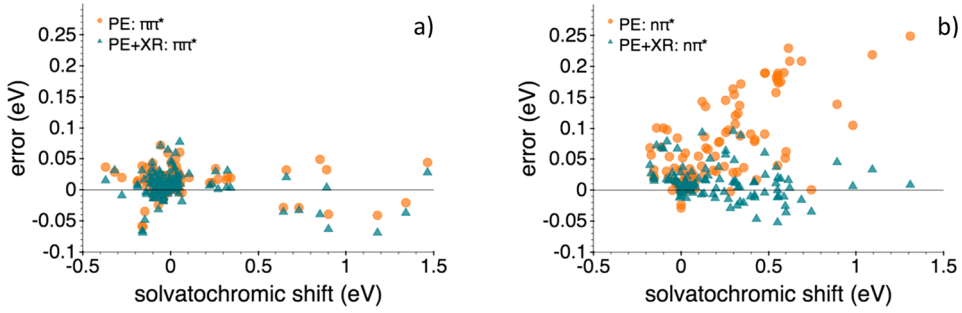

Figure 4. PE and PE + XR errors for (a) $\pi\pi^*$ and (b) $n\pi^*$ excitations as a function of the solvatochromic shift.

energies for this scheme are overestimated by a larger amount when compared to the original PE scheme. However, the main drawback of the PE + S scheme is the number of missing excitations. Out of the considered 387 full-system excitations, 89 could not be matched to any excitation computed with the PE + S scheme. This could be a consequence of significant changes in the energies and ordering of the QM orbitals upon smearing the electronic charges on the fragments. Generally speaking, Gaussian smearing results in a more favorable (energetically lowering) interaction of the electronic wave function with fragment charges. That is, the QM density tends to penetrate more into the space of the fragments. In the case of fragment−fragment interactions, charge-penetration correction leads to increase of the electrostatic component (making the Coulomb energy more stabilizing) and significant improvement of the multipole-based description of electrostatic energies.[67] This was expected to be the case for the QM/EFP interactions as well.[41] However, as revealed in the present benchmark, in general, the charge-penetration correction does not improve description of the excitation energies and solvatochromic shifts. On the contrary, the charge smearing produces a destabilizing effect on the electronic excitations and is not recommended for general use.

On the other hand, as follows from Figure 3 and Table 2, adding exchange repulsion to the QM/EFP Hamiltonian clearly improves the description of the excitation energies. In the scheme with exchange repulsion and charge-penetration correction (PE + SXR), the number of missing excitations is less than 20 and the error distribution is comparable to that of the PE scheme. However, adding only exchange repulsion to the polarizable embedding (PE + XR) seems to give the best results. This combination noticeably improves the accuracy of excitation energies, resulting in a narrow error distribution (the standard deviation of 0.034 eV) and the smallest mean (0.004 eV). For comparison, the standard deviation and mean of the PE scheme are 0.052 and 0.024 eV, respectively.

To better understand the effect of exchange repulsion on the QM/EFP excitation energies, we separately analyzed errors for the $\pi\pi^*$ and $n\pi^*$ types of excitations. According to Table 2, the MAEs for the PE and PE + XR schemes are comparable for $\pi\pi^*$ transitions. However, for $n\pi^*$ transitions, the MAE for the PE scheme is larger than the MAE for PE + XR by approximately a factor of 3. Indeed, we observe a significantly better performance of the PE + XR scheme in the case of excitations accompanied by a partial charge transfer to or from the solvent.

Note that, while excitations dominated by a charge transfer between solute and solvent are beyond the reach of most fragmentation and QM/MM models, the excitations with a small to medium amount of charge transfer are still tractable with QM/MM. Here, a transition was considered as possessing charge-transfer character if, in full quantum calculations, over 1% of the electron density corresponding to the hole or electron

https://dx.doi.org/10.1021/acs.jctc.9b01156
J. Chem. Theory Comput. 2020, 16, 6408−6417

was located on the solvent, although the value rarely exceeded 10%. We found that less than 20% of the $\pi\pi^*$ excitations involve to/from solvent charge transfer, while the charge-transfer character is present in about 70% of the $n\pi^*$ excitations.

Parts a and b of Figure 4 show the dependence of PE and PE + XR errors on the values of the solvatochromic shifts for $\pi\pi^*$ and $n\pi^*$ excitations, respectively. In the case of $\pi\pi^*$ excitations (Figure 4a), errors for both schemes are similar and do not depend on the values of the solvatochromic shifts, which are rather small for the majority of these excitations. By contrast, the PE and PE + XR schemes perform drastically differently for $n\pi^*$ excitations (Figure 4b): while the errors of the PE scheme correlate with values of the solvatochromic shifts and become as large as 0.25 eV, the errors of the PE + XR scheme remain relatively constant and do not exceed 0.1 eV. In other words, the exchange-repulsion term significantly improves the description of charge-transfer-from-solvent states with blue solvatochromic shifts. Indeed, there is a correlation between the errors in solvatochromic shifts and the amount of a hole density on a solvent, while no such correlation exists for the transfer of the electron density (see Figure S2).

An example of a solvent-to-solute charge-transfer $n\pi^*$ transition is shown in Figure 5. This excitation corresponds to

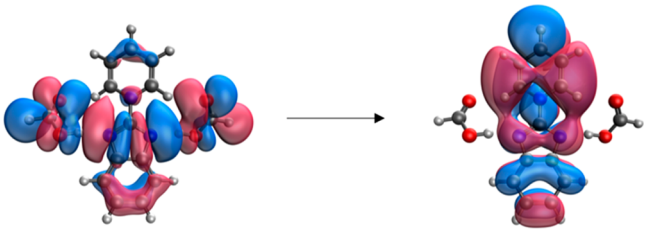

Figure 5. Example of $n\pi^*$ transition involving charge transfer from solvent to solute. This transition is the leading transition in the 11th excited state of pyridiniumyl benzimidazolide (structure **6c** in Table TS2).

the data point with the largest error in the PE scheme (0.249 eV). PE + XR decreases the corresponding error to 0.009 eV. Note that, in this electronic transition, the occupied orbital (in the fully quantum treatment) is partially delocalized over the solvent, i.e., contains basis function contributions from both the solute and solvent. Such delocalization of occupied orbitals is typical for solute *n* orbitals participating in H-bonding with solvent molecules. When an electron from such a delocalized orbital is excited to a virtual orbital localized on the solute, the transition possesses solvent-to-solute charge-transfer character. If the full system is treated quantum mechanically, delocalization of the orbital between the solute and solvent molecules can be thought of as a consequence of a resonance interaction or mixing of a pair of orbitals belonging to the solute and the solvent. As discussed in ref 84, such mixing of the occupied orbitals (so-called oo-mixing) leads to destabilization (rising in energy) of the solute orbital. On the other hand, mixing of the virtual orbitals (vv-mixing), associated with the solute-to-solvent charge transfer, results in lowering the energy of the solute orbital. Figure S3 schematically shows the orbital energy diagram in a solute−solvent system. In the case where the solvent is described classically, solute−solvent orbital mixing and associated charge transfer do not occur. However, the PE + XR scheme effectively raises (destabilizes) both occupied and virtual orbitals of the solute due to interaction of these orbitals with repulsive potentials positioned on the solvent molecules. The amount of such an orbital destabilization correlates with a spatial overlap between the solute orbital and the Gaussian functions on the solvent molecules (see Figure S3). Thus, as is observed in this work, the PE + XR scheme improves the description of the excitations with prevalent solute−solvent delocalization of the occupied orbitals because the XR term mimics the quantum effect of a solute orbital destabilization upon mixing with the solvent orbital. On the other hand, this analysis suggests that the repulsive potentials might worsen the description of the solute-to-solvent charge-transfer states (associated with mixing of the virtual orbitals), because in this case the quantum mechanical orbital mixing results in lowering the virtual solute orbital and decreasing the excitation energy while the PE + XR scheme would still tend to increase the energy of the solute virtual orbital and the excitation energy. Indeed, a small number of electronic transitions with the solute-to-solvent charge-transfer character were identified, for which the PE + XR scheme was found to be slightly less accurate than the PE scheme (see Table TS3). However, at least in the considered data set, the solute-to-solvent charge transfer occurred rarely and to a significantly smaller extent than the solvent-to-solute charge transfer, justifying the use of the PE + XR scheme. The detailed comparison of the PE and PE + XR schemes for excitations classified by their charge-transfer character is provided in Table TS3.

Detailed analyses of several excitations are provided in Table 3 and Table TS4. Table 3 shows $\pi\pi^*$ and $n\pi^*$ transitions with red and blue solvatochromic shifts. As expected, adding the exchange-repulsion term increases the energy of the orbitals when compared to the PE scheme. Despite this shift, both schemes approximate the gap between occupied and virtual orbitals well, although the PE scheme tends to have a slightly larger gap in comparison to the PE + XR scheme. From Table 3, it seems that overestimation of the gap by the PE scheme leads to larger excitation energy errors. Furthermore, there seems to exist a correlation between the gap and the solvatochromic shift; that is, when the gap estimated by the PE scheme is larger, the corresponding solvatochromic shift is more positive. Unfortunately, no analogous relations can be drawn from comparison between the PE + XR scheme and the fully quantum mechanical calculations.

The provided statistics and analysis include a large number of high-energy excited states. Now we switch to the discussion of low-lying excited states. These data are shown in the middle section of Table 2. When only the first five excited states are considered for each geometry, the mean absolute errors for the PE and the PE + XR schemes decrease from 0.035 and 0.023 eV to 0.034 and 0.017 eV, respectively. No change was observed in the mean absolute error for the excitations categorized as $\pi\pi^*$, but interestingly, the mean absolute error for the $n\pi^*$ transitions increased to 0.073 eV in the PE scheme and decreased to 0.016 eV in the PE + XR scheme. The increase in the $n\pi^*$ MAE for the PE scheme derives from excluding a large number of high excitations with small absolute errors. However, this increase is not large enough to overcome the contribution of the $\pi\pi^*$ transitions to the overall mean absolute error.

Utilizing diffuse basis sets is often essential for computing excited states, since many excitations tend to be more delocalized than the ground state. The bottom section of Table 2 presents statistics of calculations with aug-cc-pVDZ basis for the QM region. Ninety-three excitation energies were considered (excitations above the fifth state were excluded). The mean absolute errors for the PE and PE + XR schemes with the

https://dx.doi.org/10.1021/acs.jctc.9b01156
J. Chem. Theory Comput. 2020, 16, 6408−6417

Table 3. Comparison of Orbitals and Solvatochromic Shifts for Several Electronic Excitations Computed with Fully Quantum Mechanical, PE, and PE + XR Models in cc-pVDZ Basis Set[a]

Geometry/ State	Scheme	Occupied Energy	Virtual Energy	Gap	Excitation energy	Solv. shift	Occupied Orbital	Virtual Orbital
7a / 2	Gas	-10.694	1.197	11.891	5.489		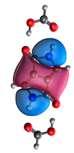	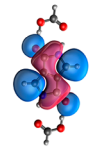
	Full QM	-10.705	0.857	11.562	5.121	-0.367		
	PE	-10.585	1.009	11.595	5.157	-0.333		
	PE+XR	-10.406	1.157	11.562	5.135	-0.355		
1a / 3	Gas	-11.230	2.136	13.366	6.009		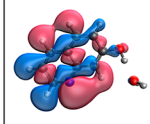	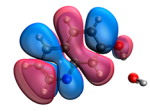
	Full QM	-10.915	2.474	13.388	6.004	-0.005		
	PE	-10.895	2.493	13.388	6.003	-0.006		
	PE+XR	-10.863	2.533	13.396	6.007	-0.001		
1x / 3	Gas	-11.135	2.123	13.258	5.883		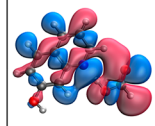	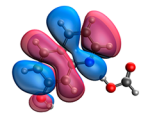
	Full QM	-11.676	1.733	13.410	6.571	0.688		
	PE	-12.221	1.772	13.992	6.779	0.896		
	PE+XR	-11.965	1.848	13.813	6.555	0.672		
6c / 2	Gas	-6.985	0.482	7.467	4.164		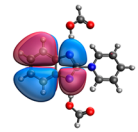	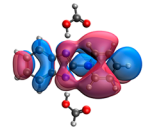
	Full QM	-7.823	0.512	8.335	5.064	0.900		
	PE	-7.750	0.539	8.289	5.025	0.861		
	PE+XR	-7.644	0.637	8.280	5.001	0.837		

[a]All energies are reported in electronvolts.

aug-cc-pVDZ basis set are 0.048 and 0.032 eV, respectively, but the values decrease to 0.031 and 0.019 eV when 30 transitions that involve transitions to Rydberg orbitals are also excluded. The MAEs for the $\pi\pi^*$ transitions are 0.020 and 0.021 eV for the PE and PE + XR schemes, while the corresponding values for the $n\pi^*$ transitions are 0.065 and 0.013 eV. Table TS3 provides a detailed analysis of orbital energies for some of the transitions analyzed with this basis set. Additionally, Table TS5 compares the PE and PE + XR schemes in cc-pVDZ and aug-cc-pVDZ bases for three characteristic $n\pi^*$ transitions. Table TS5 demonstrates the transferability of the exchange-repulsion parameters to EFP potentials created with a different basis set.

Overall, the performances of QM/EFP models in cc-pVDZ and aug-cc-pVDZ bases are similar. In both basis sets, the PE scheme is reliable for $\pi\pi^*$ transitions but becomes less accurate for $n\pi^*$ transitions, for which the PE + XR scheme is more accurate.

Out of 387 excitations considered in this benchmark, 63 could be characterized as transitions to Rydberg orbitals. Despite the initial expectation that the exchange-repulsion term would destabilize a Rydberg orbital and increase the corresponding excitation energy, over half of these energies seem to be underestimated by both PE and PE + XR schemes. By a close examination of such transitions, we observed that in most cases the exchange-repulsion term increased the energy of the valence occupied orbital by a larger amount than the energy of the Rydberg orbital. This trend could be attributed to the fact that in most transitions the Rydberg orbitals were located away from the solvent, as shown in Figure 6, and were mainly unaffected by the exchange-repulsion term. Thus, in order to determine whether the exchange-repulsion contribution to the QM/EFP Hamiltonian does in fact destabilize Rydberg orbitals and improves the description of Rydberg states, it is necessary to consider systems in which the chromophore is fully surrounded by solvent molecules. This task is left for future work. Future work will also explore the effect of exchange repulsion on the electronic properties of charged chromophores.

CONCLUSIONS

Several hybrid QM/MM models in which the solvent is described with the EFP method were introduced and benchmarked for electronic excitations of nine biologically

https://dx.doi.org/10.1021/acs.jctc.9b01156
J. Chem. Theory Comput. 2020, 16, 6408−6417

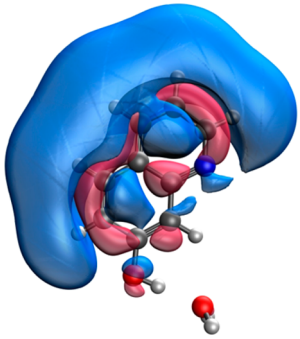

Figure 6. Example of a Rydberg orbital (structure **1a** in the Supporting Information).

relevant chromophores embedded in clusters of polar solvent molecules. All considered schemes correspond to polarizable embedding models, augmented with short-range terms introduced as one-electron contributions to the electronic Hamiltonian of the QM subsystem.

The original polarizable embedding model performs well for $\pi\pi^*$ excitation energies. This is because most of these transitions do not possess solute−solvent charge transfer character. However, in transitions with significant amounts of solvent-to-solute charge transfer, which is often the case in $n\pi^*$ excitations, the PE scheme becomes less reliable with errors proportional to the values of blue solvatochromic shifts and to the amount of the transferred charge. Fortunately, the exchange-repulsion QM/EFP term significantly improves the description of $n\pi^*$ excitations, making the overall QM/EFP description of the excited states more balanced. On the other hand, the exchange-repulsion term does not improve the accuracy of excitations with a prevalent solute-to-solvent charge-transfer character and Rydberg excitations, even though a small number of such excitations in the present data set warrants additional study. Interestingly, we found that adding the charge-penetration correction to the electrostatic term does not improve but rather deteriorates accuracy of the QM/EFP excitation energies. These conclusions remain the same when the calculations are performed with diffuse aug-cc-pVDZ basis on the QM region.

Performed benchmarks build a solid base for reliable application of QM/EFP models in photochemistry and photobiology. Further improvements in the accuracy of QM/EFP excitation energies might be achieved by explicitly accounting for interactions between electronic states and solvent polarization. Future work will also target development of the QM/EFP dispersion term, specifically analytic gradients and extensions to electronic excited states.

■ ASSOCIATED CONTENT

Supporting Information

The Supporting Information is available free of charge at https://pubs.acs.org/doi/10.1021/acs.jctc.9b01156.

Excitation energies for full system CIS, QM/EFP, and gas-phase calculations, as well as types and charge-transfer character and oscillator strengths; visual representations and coordinates of all complexes (PDF)

■ AUTHOR INFORMATION

Corresponding Author

Lyudmila V. Slipchenko − *Department of Chemistry, Purdue University, West Lafayette, Indiana 47906, United States;* orcid.org/0000-0002-0445-2990; Email: lslipchenko@gmail.com

Author

Claudia I. Viquez Rojas − *Department of Chemistry, Purdue University, West Lafayette, Indiana 47906, United States*

Complete contact information is available at: https://pubs.acs.org/10.1021/acs.jctc.9b01156

Notes

The authors declare no competing financial interest.

■ ACKNOWLEDGMENTS

C.I.V.R. and L.V.S. acknowledge support of the National Science Foundation (Grants CHE-1800505 and CHE-1450088). This research was supported in part through computational resources provided by Information Technology at Purdue University.

■ REFERENCES

(1) Callis, P. R.; Liu, T. Short range photoinduced electron transfer in proteins: QM-MM simulations of tryptophan and flavin fluorescence quenching in proteins. *Chem. Phys.* **2006**, *326* (1), 230−239.

(2) Hayashi, S.; Ohmine, I. Proton transfer in bacteriorhodopsin: structure, excitation, IR spectra, and potential energy surface analyses by an ab initio QM/MM method. *J. Phys. Chem. B* **2000**, *104* (45), 10678−10691.

(3) Isborn, C. M.; Gotz, A. W.; Clark, M. A.; Walker, R. C.; Martínez, T. J. Electronic absorption spectra from MM and ab initio QM/MM molecular dynamics: Environmental effects on the absorption spectrum of photoactive yellow protein. *J. Chem. Theory Comput.* **2012**, *8* (12), 5092−5106.

(4) Parac, M.; Doerr, M.; Marian, C. M.; Thiel, W. QM/MM calculation of solvent effects on absorption spectra of guanine. *J. Comput. Chem.* **2010**, *31* (1), 90−106.

(5) Senn, H. M.; Thiel, W. QM/MM methods for biomolecular systems. *Angew. Chem., Int. Ed.* **2009**, *48* (7), 1198−1229.

(6) Chen, J.; Martinez, T. J. QTPIE: Charge transfer with polarization current equalization. A fluctuating charge model with correct asymptotics. *Chem. Phys. Lett.* **2007**, *438* (4−6), 315−320.

(7) Damjanović, A.; Kosztin, I.; Kleinekathöfer, U.; Schulten, K. Excitons in a photosynthetic light-harvesting system: a combined molecular dynamics, quantum chemistry, and polaron model study. *Phys. Rev. E: Stat. Phys., Plasmas, Fluids, Relat. Interdiscip. Top.* **2002**, *65* (3), 031919−031919.

(8) Friesner, R. A.; Guallar, V. Ab initio quantum chemical and mixed quantum mechanics/molecular mechanics (QM/MM) methods for studying enzymatic catalysis. *Annu. Rev. Phys. Chem.* **2005**, *56*, 389−427.

(9) Froese, R. D. J.; Morokuma, K. The IMOMO and IMONM methods for excited states. A study of the adiabatic S0→ T1, 2 excitation energies of cyclic alkenes and enones. *Chem. Phys. Lett.* **1996**, *263* (3−4), 393−400.

(10) Gao, J. Hybrid quantum and molecular mechanical simulations: an alternative avenue to solvent effects in organic chemistry. *Acc. Chem. Res.* **1996**, *29* (6), 298−305.

(11) Gao, J. Methods and applications of combined quantum mechanical and molecular mechanical potentials. *Rev. Comput. Chem.* **2007**, *7*, 119−186.

(12) Gao, J.; Truhlar, D. G. Quantum mechanical methods for enzyme kinetics. *Annu. Rev. Phys. Chem.* **2002**, *53* (1), 467−505.

(13) Mordasini, T. Z.; Thiel, W. Combined quantum mechanical and molecular mechanical approaches. *Chimia* **1998**, *52* (6), 288−291.

(14) Field, M. J.; Bash, P. A.; Karplus, M. A combined quantum mechanical and molecular mechanical potential for molecular dynamics simulations. *J. Comput. Chem.* **1990**, *11* (6), 700−733.

(15) Singh, U. C.; Kollman, P. A. A combined ab initio quantum mechanical and molecular mechanical method for carrying out

simulations on complex molecular systems: Applications to the CH3Cl + Cl- exchange reaction and gas phase protonation of polyethers. *J. Comput. Chem.* **1986**, *7* (6), 718−730.
(16) Stanton, R. V.; Little, L. R.; Merz Jr, K. M. An examination of a Hartree-Fock/molecular mechanical coupled potential. *J. Phys. Chem.* **1995**, *99* (48), 17344−17348.
(17) Warshel, A.; Levitt, M. Theoretical studies of enzymic reactions: dielectric, electrostatic and steric stabilization of the carbonium ion in the reaction of lysozyme. *J. Mol. Biol.* **1976**, *103* (2), 227−249.
(18) Canfield, P.; Dahlbom, M. G.; Hush, N. S.; Reimers, J. R. Density-functional geometry optimization of the 150 000-atom photosystem-I trimer. *J. Chem. Phys.* **2006**, *124* (2), 024301−024301.
(19) Svensson, M.; Humbel, S.; Froese, R. D. J.; Matsubara, T.; Sieber, S.; Morokuma, K. ONIOM: a multilayered integrated MO+ MM method for geometry optimizations and single point energy predictions. A test for Diels- Alder reactions and Pt (P (t-Bu) 3) 2+ H2 oxidative addition. *J. Phys. Chem.* **1996**, *100* (50), 19357−19363.
(20) Vreven, T.; Morokuma, K.; Farkas, Ö.; Schlegel, H. B.; Frisch, M. J. Geometry optimization with QM/MM, ONIOM, and other combined methods. I. Microiterations and constraints. *J. Comput. Chem.* **2003**, *24* (6), 760−769.
(21) Higashi, M.; Truhlar, D. G. Combined electrostatically embedded multiconfiguration molecular mechanics and molecular mechanical method: application to molecular dynamics simulation of a chemical reaction in aqueous solution with hybrid density functional theory. *J. Chem. Theory Comput.* **2008**, *4* (7), 1032−1039.
(22) Tishchenko, O.; Truhlar, D. G. Optimizing the performance of the multiconfiguration molecular mechanics method. *J. Phys. Chem. A* **2006**, *110* (50), 13530−13536.
(23) Schwabe, T.; Olsen, J. M. H.; Sneskov, K.; Kongsted, J.; Christiansen, O. Solvation effects on electronic transitions: Exploring the performance of advanced solvent potentials in polarizable embedding calculations. *J. Chem. Theory Comput.* **2011**, *7* (7), 2209−2217.
(24) Sneskov, K.; Schwabe, T.; Kongsted, J.; Christiansen, O. The polarizable embedding coupled cluster method. *J. Chem. Phys.* **2011**, *134* (10), 104108.
(25) Steindal, A. H.; Ruud, K.; Frediani, L.; Aidas, K.; Kongsted, J. Excitation energies in solution: the fully polarizable QM/MM/PCM method. *J. Phys. Chem. B* **2011**, *115* (12), 3027−3037.
(26) Lin, H.; Truhlar, D. G. QM/MM: what have we learned, where are we, and where do we go from here? *Theor. Chem. Acc.* **2007**, *117* (2), 185−199.
(27) Ghosh, D.; Kosenkov, D.; Vanovschi, V.; Flick, J.; Kaliman, I.; Shao, Y.; Gilbert, A. T. B.; Krylov, A. I.; Slipchenko, L. V. Effective fragment potential method in Q-CHEM: A guide for users and developers. *J. Comput. Chem.* **2013**, *34* (12), 1060−1070.
(28) Ghosh, D.; Kosenkov, D.; Vanovschi, V.; Williams, C. F.; Herbert, J. M.; Gordon, M. S.; Schmidt, M. W.; Slipchenko, L. V.; Krylov, A. I. Noncovalent interactions in extended systems described by the effective fragment potential method: Theory and application to nucleobase oligomers. *J. Phys. Chem. A* **2010**, *114* (48), 12739−12754.
(29) Gordon, M. S.; Fedorov, D. G.; Pruitt, S. R.; Slipchenko, L. V. Fragmentation methods: A route to accurate calculations on large systems. *Chem. Rev. (Washington, DC, U. S.)* **2012**, *112* (1), 632−672.
(30) Gordon, M. S.; Freitag, M. A.; Bandyopadhyay, P.; Jensen, J. H.; Kairys, V.; Stevens, W. J. The effective fragment potential method: A QM-based MM approach to modeling environmental effects in chemistry. *J. Phys. Chem. A* **2001**, *105* (2), 293−307.
(31) Gordon, M. S.; Slipchenko, L.; Li, H.; Jensen, J. H. The Effective Fragment Potential: A General Method for Predicting Intermolecular Interactions. *Annu. Rep. Comput. Chem.* **2007**, *3*, 177−193.
(32) Gordon, M. S.; Smith, Q. A.; Xu, P.; Slipchenko, L. V. Accurate first principles model potentials for intermolecular interactions. *Annu. Rev. Phys. Chem.* **2013**, *64*, 553−578.
(33) Slipchenko, L. V. Effective Fragment Potential Method. In *Many-Body Effects and Electrostatics in Biomolecules*; Cui, Q., Meuwly, M., Ren, P., Eds.; CRC Press: 2016; pp 147−190.
(34) Slipchenko, L. V.; Gurunathan, P. K. Effective Fragment Potential Method: Past, Present, and Future. In *Fragmentation: Toward Accurate Calculations on Complex Molecular Systems*; Gordon, M. S., Ed.;Wiley: 2017; pp 183−208.
(35) Day, P. N.; Jensen, J. H.; Gordon, M. S.; Webb, S. P.; Stevens, W. J.; Krauss, M.; Garmer, D.; Basch, H.; Cohen, D. An effective fragment method for modeling solvent effects in quantum mechanical calculations. *J. Chem. Phys.* **1996**, *105* (5), 1968−1986.
(36) Ponder, J. W.; Wu, C.; Ren, P.; Pande, V. S.; Chodera, J. D.; Schnieders, M. J.; Haque, I.; Mobley, D. L.; Lambrecht, D. S.; DiStasio, R. A., Jr.; et al. Current status of the AMOEBA polarizable force field. *J. Phys. Chem. B* **2010**, *114* (8), 2549−2564.
(37) Cisneros, G. A.; Darden, T. A.; Gresh, N.; Pilmé, J.; Reinhardt, P.; Parisel, O.; Piquemal, J. P. Design Of Next Generation Force Fields From AB Initio Computations: Beyond Point Charges Electrostatics. In *Multi-scale Quantum Models for Biocatalysis*; Springer: 2009; pp 137−172.
(38) Piquemal, J.-P.; Cisneros, G. A.; Reinhardt, P.; Gresh, N.; Darden, T. A. Towards a force field based on density fitting. *J. Chem. Phys.* **2006**, *124* (10), 104101−104101.
(39) Grimme, S. A general quantum mechanically derived force field (QMDFF) for molecules and condensed phase simulations. *J. Chem. Theory Comput.* **2014**, *10* (10), 4497−4514.
(40) McDaniel, J. G.; Yu, K.; Schmidt, J. R. Ab initio, physically motivated force fields for CO2 adsorption in zeolitic imidazolate frameworks. *J. Phys. Chem. C* **2012**, *116* (2), 1892−1903.
(41) Gurunathan, P. K.; Acharya, A.; Ghosh, D.; Kosenkov, D.; Kaliman, I.; Shao, Y.; Krylov, A. I.; Slipchenko, L. V. Extension of the effective fragment potential method to macromolecules. *J. Phys. Chem. B* **2016**, *120* (27), 6562−6574.
(42) Stone, A. J. *The Theory of Intermolecular Forces*; Oxford University Press: Oxford, U.K., 1996.
(43) Adamovic, I.; Gordon, M. S. Dynamic polarizability, dispersion coefficient C6 and dispersion energy in the effective fragment potential method. *Mol. Phys.* **2005**, *103* (2−3), 379−387.
(44) Jensen, J. H.; Gordon, M. S. An approximate formula for the intermolecular Pauli repulsion between closed shell molecules. *Mol. Phys.* **1996**, *89* (5), 1313−1325.
(45) Ghosh, D.; Isayev, O.; Slipchenko, L. V.; Krylov, A. I. Effect of solvation on the vertical ionization energy of thymine: from microhydration to bulk. *J. Phys. Chem. A* **2011**, *115* (23), 6028−6038.
(46) Kosenkov, D.; Slipchenko, L. V. Solvent effects on the electronic transitions of p-nitroaniline: A QM/EFP study. *J. Phys. Chem. A* **2011**, *115* (4), 392−401.
(47) Slipchenko, L. V. Solvation of the excited states of chromophores in polarizable environment: Orbital relaxation versus polarization. *J. Phys. Chem. A* **2010**, *114* (33), 8824−8830.
(48) Chibani, S.; Jacquemin, D.; Laurent, A. D. Modelling solvent effects on the absorption and emission spectra of constrained cyanines with both implicit and explicit QM/EFP models. *Comput. Theor. Chem.* **2014**, *1040−1041*, 321−327.
(49) Chakraborty, R.; Bose, S.; Ghosh, D. Effect of solvation on the ionization of guanine nucleotide: A hybrid QM/EFP study. *J. Comput. Chem.* **2017**, *38* (29), 2528−2537.
(50) Sadybekov, A.; Krylov, A. I. Coupled-cluster based approach for core-level states in condensed phase: Theory and application to different protonated forms of aqueous glycine. *J. Chem. Phys.* **2017**, *147* (1), 014107.
(51) Blumberger, J. Free energies for biological electron transfer from QM/MM calculation: method, application and critical assessment. *Phys. Chem. Chem. Phys.* **2008**, *10* (37), 5651−5667.
(52) Söderhjelm, P.; Husberg, C.; Strambi, A.; Olivucci, M.; Ryde, U. Protein influence on electronic spectra modeled by multipoles and polarizabilities. *J. Chem. Theory Comput.* **2009**, *5* (3), 649−658.
(53) Tazhigulov, R.; Gurunathan, P. K.; Kim, Y.; Slipchenko, L.; Bravaya, K. B. Polarizable embedding for simulating redox potentials of biomolecules. *Phys. Chem. Chem. Phys.* **2019**, *21*, 11642−11650.
(54) Beerepoot, M. T. P.; Steindal, A. H.; Ruud, K.; Olsen, J. M. H.; Kongsted, J. Convergence of environment polarization effects in

https://dx.doi.org/10.1021/acs.jctc.9b01156
J. Chem. Theory Comput. 2020, 16, 6408−6417

multiscale modeling of excitation energies. *Comput. Theor. Chem.* **2014**, *1040*, 304−311.
(55) Slipchenko, L. V.; Gordon, M. S.; Ruedenberg, K. Dispersion interactions in QM/EFP. *J. Phys. Chem. A* **2017**, *121* (49), 9495−9507.
(56) Viquez Rojas, C. I.; Fine, J.; Slipchenko, L. V. Exchange-repulsion energy in QM/EFP. *J. Chem. Phys.* **2018**, *149* (9), 094103−094103.
(57) Kemp, D. D.; Rintelman, J. M.; Gordon, M. S.; Jensen, J. H. Exchange repulsion between effective fragment potentials and ab initio molecules. *Theor. Chem. Acc.* **2010**, *125* (3), 481−491.
(58) Zech, A.; Ricardi, N.; Prager, S.; Dreuw, A.; Wesolowski, T. A. Benchmark of Excitation Energy Shifts from Frozen-Density Embedding Theory: Introduction of a Density-Overlap-Based Applicability Threshold. *J. Chem. Theory Comput.* **2018**, *14* (8), 4028−4040.
(59) Olsen, J. M.; Aidas, K.; Kongsted, J. Excited States in Solution through Polarizable Embedding. *J. Chem. Theory Comput.* **2010**, *6* (12), 3721−3734.
(60) Guido, C. A.; Jacquemin, D.; Adamo, C.; Mennucci, B. Electronic Excitations in Solution: The Interplay between State Specific Approaches and a Time-Dependent Density Functional Theory Description. *J. Chem. Theory Comput.* **2015**, *11* (12), 5782−5790.
(61) Ren, S.; Lipparini, F.; Mennucci, B.; Caricato, M. Coupled Cluster Theory with Induced Dipole Polarizable Embedding for Ground and Excited States. *J. Chem. Theory Comput.* **2019**, *15* (8), 4485−4496.
(62) Lunkenheimer, B.; Köhn, A. Solvent Effects on Electronically Excited States Using the Conductor-Like Screening Model and the Second-Order Correlated Method ADC(2). *J. Chem. Theory Comput.* **2013**, *9* (2), 977−994.
(63) Mewes, J.-M.; You, Z.-Q.; Wormit, M.; Kriesche, T.; Herbert, J. M.; Dreuw, A. Experimental Benchmark Data and Systematic Evaluation of Two a Posteriori, Polarizable-Continuum Corrections for Vertical Excitation Energies in Solution. *J. Phys. Chem. A* **2015**, *119* (21), 5446−5464.
(64) Lin; Gao, J. Solvatochromic Shifts of the n → π^* Transition of Acetone from Steam Vapor to Ambient Aqueous Solution: A Combined Configuration Interaction QM/MM Simulation Study Incorporating Solvent Polarization. *J. Chem. Theory Comput.* **2007**, *3* (4), 1484−1493.
(65) Gao, J.; Byun, K. Solvent effects on the nπ^* transition of pyrimidine in aqueous solution. *Theor. Chem. Acc.* **1997**, *96* (3), 151−156.
(66) Ghosh, D.; Kosenkov, D.; Vanovschi, V.; Williams, C. F.; Herbert, J. M.; Gordon, M. S.; Schmidt, M. W.; Slipchenko, L. V.; Krylov, A. I. Noncovalent Interactions in Extended Systems Described by the Effective Fragment Potential Method: Theory and Application to Nucleobase Oligomers. *J. Phys. Chem. A* **2010**, *114* (48), 12739−12754.
(67) Slipchenko, L. V.; Gordon, M. S. Electrostatic energy in the effective fragment potential method: Theory and application to benzene dimer. *J. Comput. Chem.* **2007**, *28* (1), 276−291.
(68) Hohenstein, E. G.; Sherrill, C. D. Density fitting and Cholesky decomposition approximations in symmetry-adapted perturbation theory: Implementation and application to probe the nature of π-π interactions in linear acenes. *J. Chem. Phys.* **2010**, *132* (18), 184111−184111.
(69) Hohenstein, E. G.; Parrish, R. M.; Sherrill, C. D.; Turney, J. M.; Schaefer, H. F., III Large-scale symmetry-adapted perturbation theory computations via density fitting and Laplace transformation techniques: Investigating the fundamental forces of DNA-intercalator interactions. *J. Chem. Phys.* **2011**, *135* (17), 174107.
(70) Kaliman, I. A.; Slipchenko, L. V. LIBEFP: A new parallel implementation of the effective fragment potential method as a portable software library. *J. Comput. Chem.* **2013**, *34* (26), 2284−2292.
(71) Kaliman, I. A.; Slipchenko, L. V. Hybrid MPI/OpenMP parallelization of the effective fragment potential method in the libefp software library. *J. Comput. Chem.* **2015**, *36* (2), 129−135.
(72) Marefat Khah, A.; Reinholdt, P.; Olsen, J. M. H.; Kongsted, J.; Hättig, C. Avoiding Electron Spill-Out in QM/MM Calculations on Excited States with Simple Pseudopotentials. *J. Chem. Theory Comput.* **2020**, *16* (3), 1373−1381.
(73) Dziedzic, J.; Head-Gordon, T.; Head-Gordon, M.; Skylaris, C.-K. Mutually polarizable QM/MM model with in situ optimized localized basis functions. *J. Chem. Phys.* **2019**, *150* (7), 074103.
(74) Reinholdt, P.; Kongsted, J.; Olsen, J. M. H. Polarizable Density Embedding: A Solution to the Electron Spill-Out Problem in Multiscale Modeling. *J. Phys. Chem. Lett.* **2017**, *8* (23), 5949−5958.
(75) Giovannini, T.; Ambrosetti, M.; Cappelli, C. Quantum Confinement Effects on Solvatochromic Shifts of Molecular Solutes. *J. Phys. Chem. Lett.* **2019**, *10* (19), 5823−5829.
(76) Giovannini, T.; Lafiosca, P.; Cappelli, C. A General Route to Include Pauli Repulsion and Quantum Dispersion Effects in QM/MM Approaches. *J. Chem. Theory Comput.* **2017**, *13* (10), 4854−4870.
(77) Gökcan, H.; Kratz, E.; Darden, T. A.; Piquemal, J.-P.; Cisneros, G. A. QM/MM Simulations with the Gaussian Electrostatic Model: A Density-based Polarizable Potential. *J. Phys. Chem. Lett.* **2018**, *9* (11), 3062−3067.
(78) List, N. H.; Olsen, J. M. H.; Kongsted, J. Excited states in large molecular systems through polarizable embedding. *Phys. Chem. Chem. Phys.* **2016**, *18* (30), 20234−20250.
(79) Chen, X.; Gao, J. Fragment Exchange Potential for Realizing Pauli Deformation of Interfragment Interactions. *J. Phys. Chem. Lett.* **2020**, *11* (10), 4008−4016.
(80) Schmidt, M. W.; Baldridge, K. K.; Boatz, J. A.; Elbert, S. T.; Gordon, M. S.; Jensen, J. H.; Koseki, S.; Matsunaga, N.; Nguyen, K. A.; Su, S.; et al. General atomic and molecular electronic structure system. *J. Comput. Chem.* **1993**, *14* (11), 1347−1363.
(81) Gordon, M. S.; Schmidt, M. W. Advances in electronic structure theory: GAMESS a decade later. In *Theory and Applications of Computational Chemistry*; Elsevier: 2005; pp 1167−1189.
(82) Martin, R. L. Natural transition orbitals. *J. Chem. Phys.* **2003**, *118* (11), 4775−4777.
(83) Shao, Y.; Gan, Z.; Epifanovsky, E.; Gilbert, A. T. B.; Wormit, M.; Kussmann, J.; Lange, A. W.; Behn, A.; Deng, J.; Feng, X.; et al. Advances in molecular quantum chemistry contained in the Q-Chem 4 program package. *Mol. Phys.* **2015**, *113* (2), 184−215.
(84) Mao, Y.; Head-Gordon, M.; Shao, Y. Unraveling substituent effects on frontier orbitals of conjugated molecules using an absolutely localized molecular orbital based analysis. *Chemical Science* **2018**, *9* (45), 8598−8607.

https://dx.doi.org/10.1021/acs.jctc.9b01156
J. Chem. Theory Comput. 2020, 16, 6408−6417